

Quantitative assessment of biological dynamics with aggregate data

Stephen McCoy¹, Daniel McBride¹, D. Katie McCullough², Benjamin C. Calfee², Erik Zinser²,
David Talmy², and Ioannis Sgouralis^{1,*}

¹Department of Mathematics, University of Tennessee Knoxville, Knoxville, TN

²Department of Microbiology, University of Tennessee Knoxville, Knoxville, TN

*Corresponding author, isgoural@utk.edu

Abstract

We develop and apply a learning framework for parameter estimation in initial value problems that are assessed only indirectly via aggregate data such as sample means and/or variances. Our comprehensive framework follows Bayesian principles and consists of specialized Markov chain Monte Carlo computational schemes that rely on modified Hamiltonian Monte Carlo to align with summary statistic constraints and a novel elliptical slice sampler adapted to the parameters of biological models. We benchmark our methods with synthetic data on microbial growth in batch culture and test them on real growth curve data from laboratory replication experiments on *Prochlorococcus microbes*. The results indicate that our learning framework can utilize experimental or historical data and lead to robust parameter estimation and data assimilation in ODE models of biological dynamics that outperform least-squares fitting.

Keywords: Batch culture, growth curve, *Prochlorococcus*, dynamical systems, Hamiltonian Monte Carlo, statistical learning

1 Introduction

The practice of acquiring large sets of individual data points and combining them to obtain diverse summary statistics, which we refer to as data aggregation, is a prevalent technique used in multiple domains, including economics, policy making, social sciences, healthcare, and biological and ecological research [26, 63, 40]. In modern science and engineering, the interpretation of aggregate data is often preferable to the interpretation of raw data, and this practice is represented in all high-level data analysis contexts.

Specifically, in the life and biological sciences aggregate data is often generated in replication experiments where the experiment's actual raw measurements are used to generate summary statistics, such as averages and standard errors, that are maintained, curated, and made openly available while the original raw measurements are either discarded or access to them is kept restricted. This practice has the obvious advantages of conserving storage space when processing large data sets such as time-lapse and image data [31], obscuring the actual source of the data for security and privacy or competitive purposes [66, 20], reducing noise [68, 16], and aiding comparison between different experiments or protocols that are probing the same system but employing different modalities [67]. However, such practice leads to data collection problems, for example having only summary statistics and having difficulty acquiring raw data for a complete understanding of Covid-19 data affected maternal and neonatal outcomes [59]. An additional challenge, perhaps more significant, of working with pre-processed data is the loss of information that occurs when generating it [49] and also the loss of reference to the underlying specific biological processes [56].

Data aggregation also poses serious challenges with rigorous data analysis or assimilation techniques [30]. Specifically, within data assimilation, the goal is to develop mathematical frameworks that process information available in empirical form and obtain quantitative predictions [65]. However, predictions following the assimilation of aggregated data are limited by lost information or distortions caused by aggregation [22, 15]. In order to counteract such artifacts, elaborate frameworks that combine domain knowledge and physical constraints in the form of specialized models are often required. Such approaches naturally lend themselves to Bayesian assimilation methodologies [53].

Bayesian data assimilation methods have seen an increase in popularity, particularly in parameter estimation applications for dynamical problems modeled with initial value problems (IVP) [24, 23, 36]. A major advantage is that they offer uncertainty quantification, as the standard practice is to learn an entire distribution of plausible values for every variable of interest rather than point estimators. Another advantage is that they can restrict the parameters under estimation to only meaningful values; for instance, a rate parameter or an initial population can be assigned a prior distribution with only positive support, or prior distributions can be defined on only the intervals that remain meaningful in the scales of the underlying problem. Furthermore, they distinguish identifiable and nonidentifiable cases, the distinction of which is a common modeling challenge in mathematical biology [38, 64]. Finally, they offer modeling flexibility and realism that comes from explicitly accounting for different sources of noise and complexity characteristic of the systems being studied [51].

Nevertheless, Bayesian data assimilation is not without its drawbacks, especially for IVPs. To start, one needs to

construct and characterize, often via intensive computational sampling procedures, the relevant posterior distribution. In particular, in the parameter estimation problem of ODE models, this involves numerically integrating the ODE for each new configuration of parameters for each sample [46, 55, 1]. Given that required sample sizes are typically large, sampling strategies become computationally costly and require efficient computational algorithms that are the topic of ongoing research. In addition, biological dynamics are typically contaminated with multiplicative noise [12, 13, 23] which poses additional challenges to many existing algorithms which assume additive noise. Furthermore, the predictions provided in Bayesian data assimilation depends critically on the model used, its fidelity to the modeled system, and the quality of the data supplied.

A particular challenge when training a dynamical model with aggregated data is that, to properly model the data points that give rise to the supplied summary statistics, we have to mathematically reproduce the collapsing of unavailable raw measurements down to the available values. In the statistical representation of the resulting model, this translates into fitting the model parameters with *singular distributions*, that is, probability distributions supported only on subspaces of lower dimension than the model's full parameter space. Parameter estimation is a routine topic in the Bayesian literature focused on simple models with nonsingular distributions [58, 51]; however, parameter estimation with singular distributions under complex statistical models necessary to tackle real-world biological scenarios remains an open challenge.

In this study, we develop a novel comprehensive statistical learning framework that addresses these challenges. Our framework allows for parameter estimation in IVPs of ODE models and also allows modeling of the latent raw measurements that gave rise to the summary statistics forming our dataset. To perform parameter estimation on our statistical model, we apply methods that can sample from distributions restricted to particular subsets of the parameter space as determined by data aggregation. To this end, we develop a novel extension of the Hamiltonian Monte Carlo (HMC) sampling algorithm that allows for navigating highly dimensional parameter spaces while accounting for parameter constraints.

The rest of this study is structured as follows. In **METHODS**, we begin by describing the data set under consideration, the IVP we aim to address, and the Bayesian framework used for parameter estimation. First, we present the Bayesian framework in general form, followed by its application to the analysis of growth curve data. In **RESULTS**, we demonstrate how our framework performs and compare it with *in silico* and *in vitro* data of microbial growth curves from batch culture experiments commonly conducted in microbiology. Lastly, in **DISCUSSION**, we provide an overview of our methods and elaborate on its perspectives for future applications.

2 Methods

In this section, we first present a general description of our framework that emphasizes modeling and computational aspects. Subsequently, we present a specialized application to microbial growth curves obtained in replication experiments.

2.1 Statistical learning

2.1.1 Learning scheme

Our framework considers the analysis of aggregated data that we denote by $z_{1:N}^{1:M}$. Specifically, we denote individual data points with z_n^m and use superscripts $m = 1, \dots, M$ to refer to different summary statistics that may be available and subscripts $n = 1, \dots, N$ to refer to assessments made at time t_n . For example, z_{2}^1 indicates our 1st summary statistic obtained at the 2nd time assessment.

Our data stem from collapsing batches of raw measurements made at the same time, which we represent by

$$z_n^m = G^m(y_n^{1:K}). \quad (1)$$

Here, y_n^k denote individual raw measurements, made at time t_n , and $k = 1, \dots, K$ indexes the batch of measurements. The functions $G^m(\cdot)$ model the corresponding batch statistics. For instance, the common sample mean and variance correspond to the functions

$$G^1(y^{1:K}) = \frac{1}{K} \sum_{k=1}^K y^k, \quad (2)$$

$$G^2(y^{1:K}) = \frac{1}{K-1} \sum_{k=1}^K \left(y^k - \frac{1}{K} \sum_{k'=1}^K y^{k'} \right)^2. \quad (3)$$

In this study, we focus on the cases where *only* $z_{1:N}^{1:M}$ are available, while $y_{1:N}^{1:K}$ are *not*. For this reason, we explicitly model the missing measurements using a likelihood that represents biological or measurement noise. Our likelihood

$$y_n^k | g, h \sim \mathbb{A}(F(x^g(t_n)), h) \quad (4)$$

is a probability distribution that models the generation of independent measurements. Here, $F(\cdot)$ is a problem-specific observation function that links measurements with the dynamical variables $x^g(\cdot)$ of an underlying ordinary differential equation (ODE) that models the dynamics of interest. Often, this is simply a projection that reduces the full dynamical state of the system of interest to a single component. The parameter h allows for tunable noise characteristics, such as noise spread, which can better reflect the inherent statistics of the measurements.

To model the dynamics of our system, we consider a generic initial value problem (IVP) for an ODE of the form

$$\frac{dx}{dt} = H^g(t, x). \quad (5)$$

The function dynamics $H^g(\cdot, \cdot)$ is also problem specific and depends on unknown parameters g . Together, with the appropriate initial conditions that may also depend on unknown parameters g , our IVP leads to a solution $x^g(t)$ which, at any time t , describes the dynamical state of the system of interest.

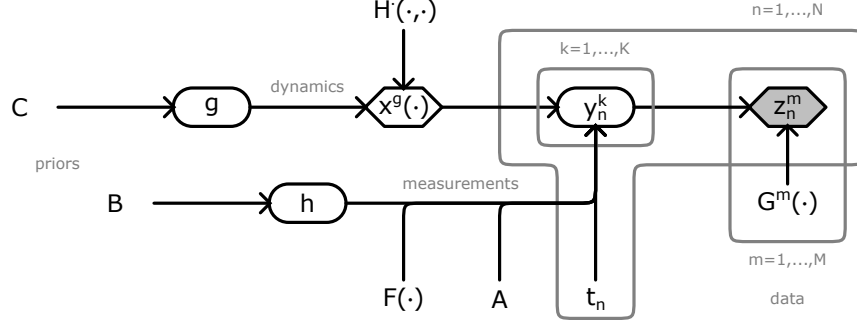


Figure 1: Graphical representation of the statistical learning framework in this study. Following the common convention, random quantities are shown with circles, deterministic quantities are shown with diamonds, and quantities with known values are shaded. In addition, arrows indicate dependencies among the various quantities of interest, plates indicate repetition over the marked index, and hyperparameters are left free.

Our framework contains unknown measurements $y_{1:N}^{1:K}$ whose statistical properties are fully described by the likelihood in eq. (4) and also unknown parameters g and h . The latter affects the noise of the system, while the former affects the dynamics. Following the Bayesian paradigm [51], we assign priors to them

$$h \sim \mathbb{B}, \quad (6)$$

$$g \sim \mathbb{C}, \quad (7)$$

which, besides completing our statistical framework, allow the specification of meaningful bounds for their values.

Given a data set $z_{1:N}^{1:M}$, assessment times $t_{1:N}$, statistics $G^{1:M}(\cdot)$, and batch size K , our learning framework consists of problem-specific choices for the noise distribution $\mathbb{A}(\cdot, \cdot)$, noise parameter h , observable $F(\cdot)$, dynamical variables g , dynamics $H(\cdot, \cdot)$, and prior distributions \mathbb{B}, \mathbb{C} . A graphical summary is shown in fig. 1 and a complete statistical summary is given in appendix A.

Once such choices are made, our framework leads to a posterior probability distribution which, via Bayes' rule [18, 32], is formally characterized by a probability density that takes the form

$$\mathcal{P}(h, g, y_{1:N}^{1:K} | z_{1:N}^{1:M}) \propto \mathcal{P}(z_{1:N}^{1:M} | y_{1:N}^{1:K}) \mathcal{P}(y_{1:N}^{1:K} | g, h) \mathcal{P}(h) \mathcal{P}(g).$$

According to our model's statistical representation, this density specializes to

$$\mathcal{P}(h, g, y_{1:N}^{1:K} | z_{1:N}^{1:M}) \propto \left[\prod_{n=1}^N \left(\prod_{m=1}^M \delta_{G^m(y_n^{1:K})}(z_n^m) \right) \left(\prod_{k=1}^K A(y_n^k | g, h) \right) \right] B(h) C(g). \quad (8)$$

Here, the factors containing Dirac deltas $\delta_{G^m(\cdot)}(\cdot)$ arise because of eq. (1), which dictate precise agreement between our model measurements and the corresponding batch statistics, while $A(\cdot | \cdot, \cdot), B(\cdot), C(\cdot)$ are the probability densities associated with the distributions $\mathbb{A}(\cdot, \cdot), \mathbb{B}, \mathbb{C}$.

2.1.2 Markov chain Monte Carlo

Due to the IVP, which most often remains analytically intractable, we generally cannot obtain a closed-form expression to the posterior of eq. (8). For this reason, to characterize eq. (8), we develop a specialized Markov chain Monte Carlo (MCMC) sampling scheme that generates pseudorandom samples of the model unknowns $h, g, y_{1:N}^{1:K}$ [37, 54, 42].

Because of the natural grouping of our unknowns, we use a *Gibbs sampler* that iterates the following two steps:

- update *parameters* by sampling from $\mathcal{P}(h, g | y_{1:N}^{1:K}, z_{1:N}^{1:M})$,
- update *measurements* by sampling from $\mathcal{P}(h, y_{1:N}^{1:K} | g, z_{1:N}^{1:M})$.

To initialize our sampler, we directly sample h and g from the priors \mathbb{B} and \mathbb{C} , respectively. Next, we sample $y_n^k | g, h$, from \mathbb{A} , and then apply root-finding on the generated $y_{1:N}^{1:M}$ to ensure that the constraints are satisfied. In all cases, we combine our sampler with appropriate numerical integrators for the solution of the IVP [52, 60, 3, 57] adapted to the specifics of the problem at hand.

In the special case where \mathbb{A} and \mathbb{B} are conditionally conjugate, our Gibbs updates can be implemented via ancestral sampling [7, 37, 18, 51] based on the factorizations

$$\begin{aligned}\mathcal{P}(h, g | y_{1:N}^{1:K}, z_{1:N}^{1:M}) &= \mathcal{P}(h | g, y_{1:N}^{1:K}) \mathcal{P}(g | y_{1:N}^{1:K}), \\ \mathcal{P}(h, y_{1:N}^{1:K} | g, z_{1:N}^{1:M}) &= \mathcal{P}(h | g, y_{1:N}^{1:K}) \mathcal{P}(y_{1:N}^{1:K} | g, z_{1:N}^{1:M}),\end{aligned}$$

both of which allow for direct sampling of h via $\mathcal{P}(h | g, y_{1:N}^{1:K})$. For both the parameters and the measurements, our updates are derived from specialized samplers adapted to $\mathcal{P}(g | y_{1:N}^{1:K})$ and $\mathcal{P}(y_{1:N}^{1:K} | g, z_{1:N}^{1:M})$ as described below.

mESS for parameter sampling The first Gibbs update requires the sampling of g from $\mathcal{P}(g | y_{1:N}^{1:K})$, which we achieve using a novel multiplicative elliptical slice sampler (mESS), which naturally aligns with distributions restricted to positive support as often found in dynamical systems of biological processes. See appendix C.1 for a detailed explanation of the sampler. Our approach retains the core benefits of elliptical slice sampling, such as parameter updates without tuning and efficient exploration of complex posterior landscapes, while offering a targeted enhancement for distributions with strictly positive values and non-Gaussian architecture [51, 47].

cHMC for measurement sampling In our second Gibbs update, we generate samples of $y_{1:N}^{1:K}$ given known parameters g and h that satisfy the constraints $z_n^m = G^m(y_n^{1:K})$ of eq. (1). For this, we apply a novel constrained Hamiltonian Monte Carlo (cHMC) method specialized for handling the constraints. Our method is fully detailed in appendix C.3. As we explain in appendix C.2, standard HMC is suitable for sampling smooth high-dimensional distributions with full support [37, 8, 5]; however, satisfying the constraints requires modifications. Our novel cHMC sampler takes advantage of the RATTLE integrator [2, 9, 21] in the HMC integration loop to ensure that the Monte Carlo samples of $y_{1:N}^{1:K}$ satisfy the constraints while remaining statistically correct, i.e. maintaining that the MCMC chain converges to the target distribution. Our method maintains HMC's efficient sampling of high-dimensional distributions [37, 8, 5] arising due to multiple time points and large batch-sizes, while permitting navigation on the support of singular distributions arising due to the constraints.

2.2 Application to Prochlorococcus growth curve data

In this section, we specialize our statistical learning framework in a case study of interest in microbiology and marine biology. In our study, the aggregated data stem from batch growth experiments of the marine cyanobacteria *Prochlorococcus* (*Pro*). *Pro* is the most abundant photosynthetic phytoplankton in the ocean [50] and is studied *in situ* for genetic and physical connections to their bio-geographical significance [17, 4]. These photosynthetic organisms play a vital role in the regulation of ocean food chains and climate [6, 50]. Laboratory growth experiments take the form of replicate time series data, where multiple sets of triplicate test tubes of *Pro* are monitored for cell density as they grow in batch culture. Data aggregation is applied to the runs to produce sample averages and variances.

Our growth curves depend on two pivotal quantities: the maximum growth rate, typically reported in units of 1/days, and the nutrient affinity, typically reported in units $m^3/(\text{cell} \cdot \text{days})$, of the *Pro* cells which we denote with m and a , respectively. These parameters, as well as the initial nutrient and *Pro* cell densities of batch culture experiments, which we denote with Q and P , determine the overall dynamics of the cell and nutrient density.

To model the dynamics in eq. (5) we introduce an IVP that consists of

$$\frac{dq}{dt} = -\frac{q}{q + \frac{m}{a}} mp \quad q(t_0) = Q \quad (9)$$

$$\frac{dp}{dt} = +\frac{q}{q + \frac{m}{a}} mp \quad p(t_0) = P \quad (10)$$

for some fixed initial time t_0 . Our dynamical state $x = (q, p)$ consists of the density of nutrients q and the density of cells p , both reported in cells/m^3 . Our eqs. (9) and (10) depend on the unknown parameters $g = (P, Q, m, a)$. Given g , we denote the solution of our IVP with $x^g(t) = (q^g(t), p^g(t))$.

In a typical experiment that monitors the growth curve, the measurements probe only the cell density. Accordingly, our measurement function in eq. (4) reduces to a projection

$$F(q, p) = p. \quad (11)$$

Theoretical and empirical studies on microbial growth [12, 13, 23] indicate the presence of multiplicative noise in the measurements. Accordingly for the likelihood $\mathbb{A}(\cdot, \cdot)$ we choose the LogNormal distribution

$$y_n^k | g, h \sim \text{LogNormal}(p^g(t_n), h) \quad (12)$$

with an unknown scale parameter h . For the definition, see appendix B.

Following section 2.1.1, we denote by y_n^k the k^{th} measurement made at time t_n during the experiment and assume the statistics in eqs. (2) and (3) to form the reported mean z_n^1 and variance z_n^2 of each time point.

Finally, for eq. (6), we apply a prior on the parameters $g = (P, Q, m, a)$ of our IVP that allows only for strictly

positive values as defined by

$$Q \sim \text{Gamma}\left(\phi_Q, \frac{\psi_Q}{\phi_Q}\right), \quad (13)$$

$$P \sim \text{Gamma}\left(\phi_P, \frac{\psi_P}{\phi_P}\right), \quad (14)$$

$$m \sim \text{Gamma}\left(\phi_m, \frac{\psi_m}{\phi_m}\right), \quad (15)$$

$$a \sim \text{Gamma}\left(\phi_a, \frac{\psi_a}{\phi_a}\right). \quad (16)$$

and, for eq. (7), we also apply a Gamma prior

$$h \sim \text{Gamma}\left(\phi_h, \frac{\psi_h}{\phi_h}\right), \quad (17)$$

which is conditionally conjugate to the likelihood in eq. (12). Here we use the parameterization of the Gamma distribution shown in appendix B.

Our framework leads to the derivation of a posterior density

$$\mathcal{P}(h, Q, P, m, a, y_{1:N}^{1:K} | z_{1:N}^{1:M}) \propto \mathcal{P}(Q)\mathcal{P}(P)\mathcal{P}(m)\mathcal{P}(a) \int_h dh \mathcal{P}(z_{1:N}^{1:M}, h | Q, P, m, a, y_{1:N}^{1:K}) \quad (18)$$

here we marginalize the noise parameter h since its value is of little biological interest. By this marginalization, we also avoid the ancestral sampling step in our MCMC implementation of section 2.1.2.

2.3 Data acquisition

The *in vivo* data shown in RESULTS are obtained with the following methodology. Axenic cultures of *Prochlorococcus* strain MIT9215 cyanobacteria were maintained in an artificial seawater medium, AMP-MN [11], a derivative of AMP-A medium [44, 43] without any nitrogen amendment. Purity tests to determine the axenicity of cyanobacteria stocks and experimental cultures were performed routinely as previously described in [45]. All experiments were carried out at 24°C in Percival I36VLX incubators (Percival, Boone, IA) with modified controllers that allowed for gradual increase and decrease of cool white light to simulate sunrise and sunset with peak midday light intensity of 150 $\mu\text{mol quanta m}^{-2}\text{s}^{-1}$ on a 14 hr:10 hr light:dark cycle [69]. The abundance of cyanobacteria was quantified by flow cytometry using a Guava EasyCyte 8HT flow cytometer (Millipore, Burlington, MA) with populations of *Prochlorococcus* determined by their red fluorescence [45, 14]. Raw measurements were obtained in batches of size $K = 24$ for a total of $N = 9$ time points spread over the duration of the experiment.

3 Results

In this section, we show how our modeling framework performs on estimating the parameters of IVPs. To demonstrate its effectiveness in revealing the correct parameter values, we first validate our model on synthetic

data mimicking real ones that are generated with prescribed parameter values. Our *in silico* data are obtained by simulating the model of section 2.2. Subsequently, we demonstrate that our methods maintain their performance on real data. Our *in vitro* data are acquired as described in section 2.3. We also compare against naive parameter estimation methods based on least-squares fitting.

3.1 In silico growth curve data

To generate the synthetic data, we employ the IVP in eqs. (9) and (10) modeling Pro growth with the ground-truth parameter values $(P, Q, m, a) = (13, 13 \times 10^4, 2, 55 \times 10^{-6})$ which we chose in agreement with the *in vitro* data of the next section. Then, we generate cell density measurements $y_{1:N}^{1:K}$ according to eq. (12) and derive summary statistics $z_{1:N}^{1:M}$ calculated by eqs. (2) and (3). Our data are shown in fig. 2 with the upper panels corresponding to a scenario in which only batch means are maintained and the lower panels to a scenario where both batch means and variances are maintained after aggregation. We then employ our statistical learning framework to generate samples of the posterior distribution considering only sample means $p(P, Q, m, a | z_{1:N}^1)$ or sample means and variances $p(P, Q, m, a | z_{1:N}^2)$.

To allow for comparison with ground truth, for each case, we approximate the maximum a posterior estimate (MAP) of our parameters by selecting the MCMC sample with the highest posterior probability density calculated by eq. (18), [62]. These estimates represent our framework's best choices for parameter values in each case and are indicated by solid lines in fig. 2. Their specific values are $(\hat{P}, \hat{Q}, \hat{m}, \hat{a}) = (13.58, 13.08 \times 10^4, 2.21, 54.80 \times 10^{-6})$ for the first case considering only batch means and $(\hat{P}, \hat{Q}, \hat{m}, \hat{a}) = (13.33, 12.89 \times 10^4, 1.89, 54.73 \times 10^{-6})$ for the second case considering both batch means and variances. Both estimators are in good agreement with the ground truth.

For the two panels in the left column of fig. 2, we also show a collection of sample trajectories. These are randomly selected MCMC samples that correspond to the solutions of eqs. (9) and (10). For both cases, we get a spread of trajectories around the MAP solution that indicates uncertainty coming from the assumed noise in the measurements and missing information due to data aggregation. The uncertainty in the upper left panel is higher than that in the lower left panel, as indicated by the wider spread of the sampler trajectories around MAP. This is expected behavior because we assimilate the same information (i.e. batch means) plus additional information (i.e. batch variances) in the second case.

The two panels in the right column of fig. 2 show MCMC samples of the parameters. Specifically, along the diagonals, we show the MCMC approximations (histograms) of the marginal posteriors $p(Q | z_{1:N}^1), p(P | z_{1:N}^1), p(m | z_{1:N}^1), p(a | z_{1:N}^1)$ along with the MAP estimates as vertical lines. Again, although there is general agreement with the ground truth, there is more uncertainty in the case of only the batch mean than in the case of both batch mean and variance, as indicated by wider histograms. In the off-diagonal panels, we show MCMC approximations (scatter plots) of each pairing of the sample parameters. In both cases, our framework reveals preferences between combinations of parameters, indicating that, to comply with the supplied data, trajectories of the underlying IVP require specific values. For instance, the pair (Q, a) has the highest correlation among all pairs. This is expected behavior, as our dynamical model, see eqs. (9) and (10), exhibits a degree of nonidentifiability between the initial

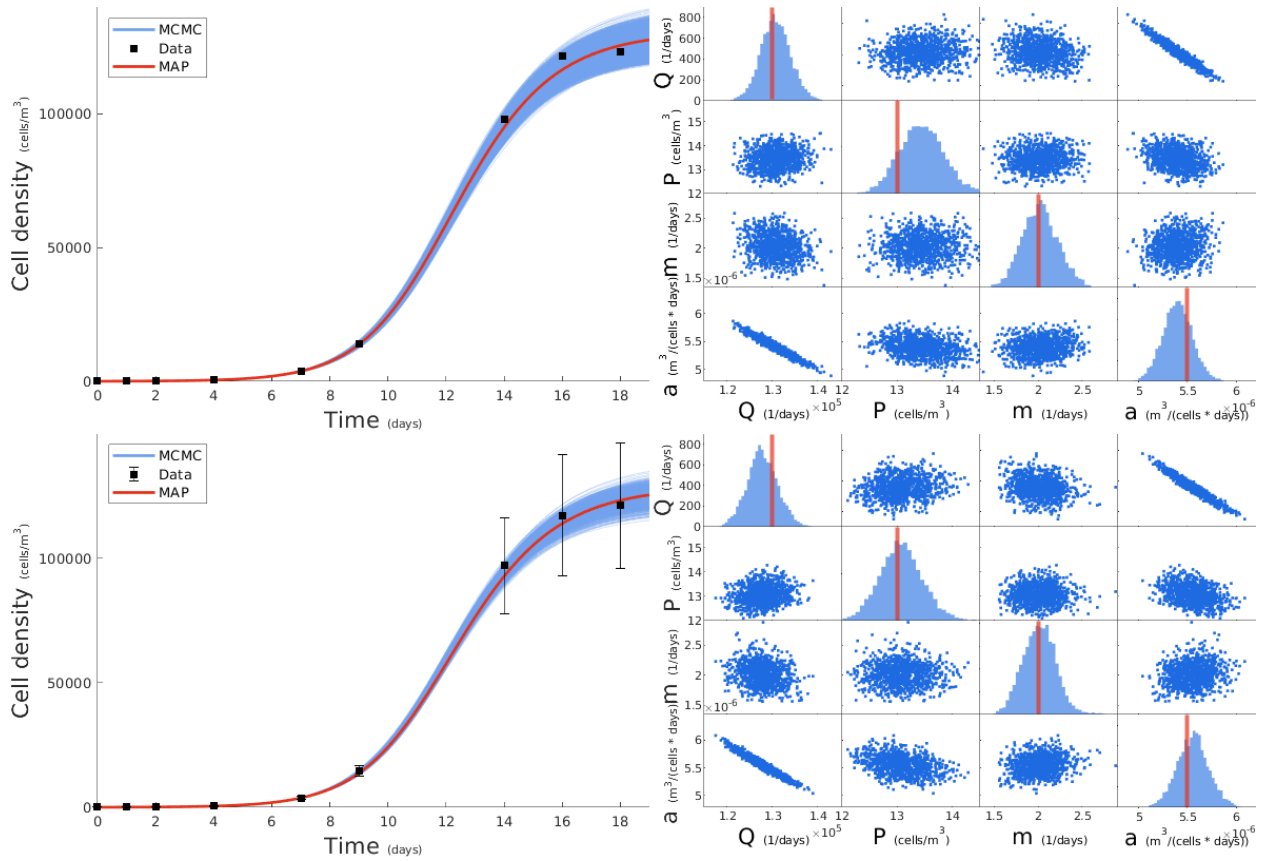


Figure 2: Fitting the synthetic data with our statistical learning framework. The first row shows our results for a linear (mean only) constraint, and the second row shows our results for a quadratic (mean and variance) constraint. (top and bottom left) We use our MCMC sampled parameter values to generate thousands of ODE solutions which are plotted as the blue curves, we then use the MAP estimate to generate the red curve and all this is compared to the data points shown as black squares. (top and bottom right) while doing the parameter estimation we can also see how well we reproduce the hidden measurements. We show scatter plots of each parameter compared with the other in the off-diagonal panels. On the diagonal panels we show the histogram created by thousands of MCMC samples of each parameter and overlay via the red vertical line the ground truth parameter value that was used to generate the synthetic data. Here our results show good performance recovering the parameter values and therefore producing a well-fitting ODE solution.

	Units	Ground truth	Only batch means		Both batch means and variances		Least squares	
$K = 24$			Estimate	% Error	Estimate	% Error	Estimate	% Error
P	cells/ m^3	13×10^4	12.95×10^4	0.42	13.43×10^4	3.34	10.43×10^4	19.75
Q	1/days	13	13.15	1.15	12.77	1.81	0.021	99.84
m	1/days	2	1.83	8.33	2.02	1.13	0.308	84.6
a	$m^3/(\text{cells} \cdot \text{days})$	5.5×10^{-6}	5.51×10^{-6}	0.24	5.33×10^{-5}	3.00	5.10×10^{-6}	189.10
$K = 12$			Estimate	% Error	Estimate	% Error	Estimate	% Error
P	cells/ m^3	13×10^4	13.52×10^4	3.97	13.52×10^4	0.633	11.92×10^4	8.28
Q	1/days	13	12.45	4.23	12.45	7.08	4.25	67.31
m	1/days	2	1.81	9.73	1.81	2.52	4.20	110.0
a	$m^3/(\text{cells} \cdot \text{days})$	5.5×10^{-6}	5.27×10^{-6}	4.26	5.27×10^{-6}	0.954	6.50×10^{-6}	18.18
$K = 6$			Estimate	% Error	Estimate	% Error	Estimate	% Error
P	cells/ m^3	13×10^4	12.32×10^4	5.22	13.77×10^4	5.96	12.48×10^4	4.02
Q	1/days	13	13.08	0.627	13.02	0.124	4.59	64.70
m	1/days	2	1.87	5.68	2.00	0.193	8.93	17.45
a	$m^3/(\text{cells} \cdot \text{days})$	5.5×10^{-6}	5.69×10^{-6}	3.40	5.22×10^{-6}	5.07	6.46×10^{-6}	17.45
$K = 3$			Estimate	% Error	Estimate	% Error	Estimate	% Error
P	cells/ m^3	13×10^4	11.80×10^4	9.21	12.86×10^4	1.11	14.30×10^4	10.03
Q	1/days	13	30.56	135.11	34.46	165.07	63.84	391.08
m	1/days	2	2.008	0.424	2.01	0.620	18.0	800.0
a	$m^3/(\text{cells} \cdot \text{days})$	5.5×10^{-6}	5.94×10^{-6}	8.09	5.75×10^{-6}	4.58	3.90×10^{-6}	29.09

Table 1: Quantitative validation against ground truth. The comparison shows that our model has better agreement with the ground truth than least squares, particularly as batch size K size decreases.

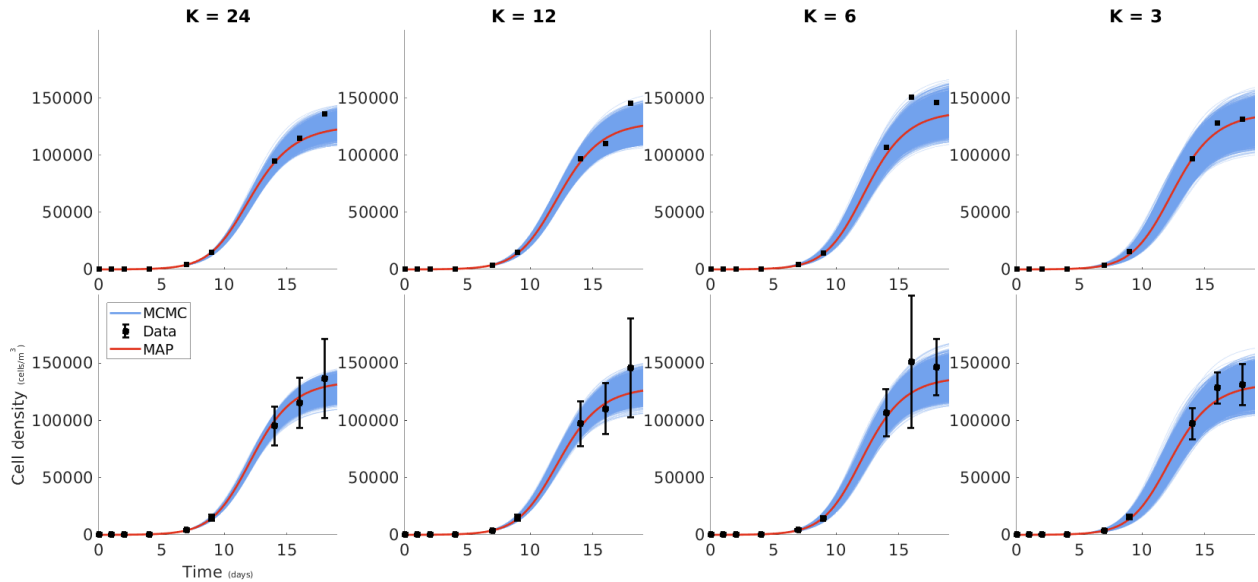
amount of nutrients and nutrient affinity.

In addition to showing that our framework successfully recovers the values of the ground truth parameters with quantified uncertainty, in fig. 3 we demonstrate the strength of our methods when challenged with scenarios involving more demanding data. To this end, we apply our learning framework on the same two cases (only batch mean and both batch mean and variance) by now considering scenarios of decreasing batch size $K = 24, 12, 6, 3$. In this way, we simulate a series of aggregate data generated in experiments of successively fewer raw measurements. Although fewer raw measurements result in increasingly noisier aggregate data, as seen in fig. 3 (upper two rows), our framework’s estimates remain in good agreement with the ground truth.

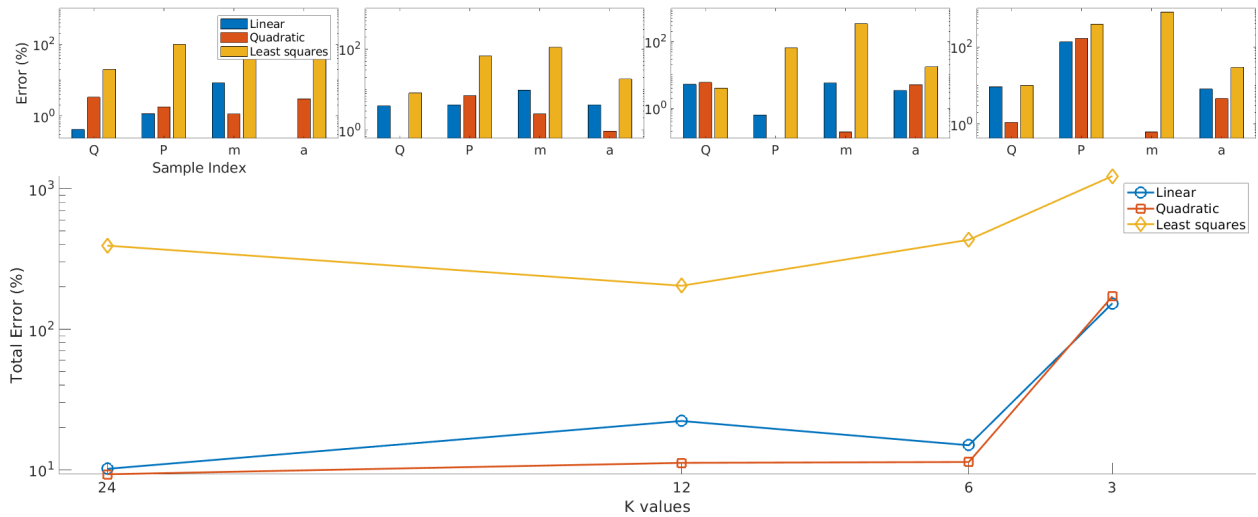
A head-to-head comparison with naive parameter estimation procedures mediated by least-square fitting (LS), see appendix D, indicates superior performance. In particular, in fig. 3 (bottom two rows) and table 1 we quantify the error percentage in our MAP estimates and those resulting from LS for each parameter $X = Q, P, m, a$ using

$$\%Error = \left(\frac{X^{\text{estimate}}}{X^{\text{ground}}} - 1 \right) \times 100\%.$$

While the error for all three methods increases as batch size K decreases, and so the noise persisting in the aggregated data increase, LS consistently produces the least accurate estimates. This indicates that, in addition to recovering the ground truth more accurately, our learning framework is also more robust when faced with excessively noisy data.



(a) Data set size effect on IVP solutions



(b) Data set size effect on error

Figure 3: Batch size robustness of our methods. We show the effect of reducing the batch size K from 24 to 3 going from left to right across all figures. In the upper two rows, we show the solutions of our IVP eqs. (9) and (10) for the linear constraints of the batch mean (top) and the quadratic constraint of the batch mean and variance (bottom) as K is decreased. In the bottom two rows, we show the percentage error between the linear constraint MAP predictions (blue), quadratic constraint MAP prediction (red), and a LS prediction (yellow) for the parameter values (P, Q, m, a) compared to their ground truth. This is shown in the upper panels as their individual errors in the form of a bar chart and in the bottom panel as a line plot of the total error (sum of individual errors) for each batch size. As we reduce the number of samples per time point down from a collection of experiments $K = 24$, to one experiment $K = 3$ we see the least squares method break down whereas our method is better at handling the decrease in the signal to noise. See table 1 in appendix D for a table of the values used in the least squares comparison.

3.2 In vitro growth curve data

Having demonstrated our framework’s ability to accurately recover ground-truth parameter values with synthetic data, we now demonstrate its application on real laboratory data. Here, our summary statistics $z_{1:N}^{1:M}$ are obtained directly from the batch growth *Pro* data. Our data are shown in fig. 4 and, as previously, we distinguish a case that considers only batch means (upper panels) and one that considers both batch means and variances (lower panels). For the two cases, our MAP estimators are $(\hat{P}, \hat{Q}, \hat{m}, \hat{a}) = (30.89, 12.45 \times 10^4, 1.94, 57.43 \times 10^{-6})$ and $(\hat{P}, \hat{Q}, \hat{m}, \hat{a}) = (53.16, 12.13 \times 10^4, 1.85, 55.51 \times 10^{-6})$, respectively. These represent growth rate estimates in line with the empirical literature (c.f. Figure 2 of [41], Figure S5 of [27]). In addition to MAP estimates, our framework fully quantifies uncertainty in this case in either trajectories or parameter values. As anticipated, our learning framework also performs well with real *Pro* experimental data.

3.3 Sensitivity analysis

Our Bayesian framework depends on prior probability distributions, which may influence our posterior estimates. To test the effect of our prior’s influence on the resulting estimates, we conduct a sensitivity analysis taking into account changes in the hyperparameters of eqs. (13) to (16). Specifically, we vary the expected values of the prior represented by $\psi_Q, \psi_P, \psi_m, \psi_a$ within $\pm 10\%$ of their baseline and obtain the resulting marginal posteriors $p(Q|z_{1:N}^{1:M}), p(P|z_{1:N}^{1:M}), p(m|z_{1:N}^{1:M}), p(a|z_{1:N}^{1:M})$ over the individual parameters. As shown on fig. 5 (upper panels), hyperparameter changes are not transmitted to the resulting posteriors, indicating that parameter point estimates are robust with respect to the model’s hyperparameters. In addition, a quantitative comparison of the estimated trajectories $p^g(\cdot)$ via the relative root-mean-square error

$$\text{RMSE} = \sqrt{\frac{1}{N} \sum_n \left(\frac{p^g(t_n)}{z_n} - 1 \right)^2},$$

also shown on fig. 5 (lower panel), illustrates that hyperparameter changes are not transmitted to the trajectories as well, indicating that our recovered dynamics are informed by the supplied data rather than the hyperparameter choices.

4 Discussion

We present a unified statistical learning approach to parameter estimation of IVPs probed with aggregated data. Our framework reproduces the missing measurements and explicitly accounts for data aggregation, this way allowing for high modeling fidelity and improved estimation. For this task, we derived and applied specialized MCMC methods, such as cHMC and mESS, that included a modified HMC algorithm to handle summary statistics constraints in the batch data we model, as well as a modified elliptical slice sampler to navigate parameter sampling [5, 48, 47, 10].

This study focuses on the analysis of biological data derived from replication measurements as commonly used in biology research. We demonstrated that our methods successfully analyze data from laboratory batch growth

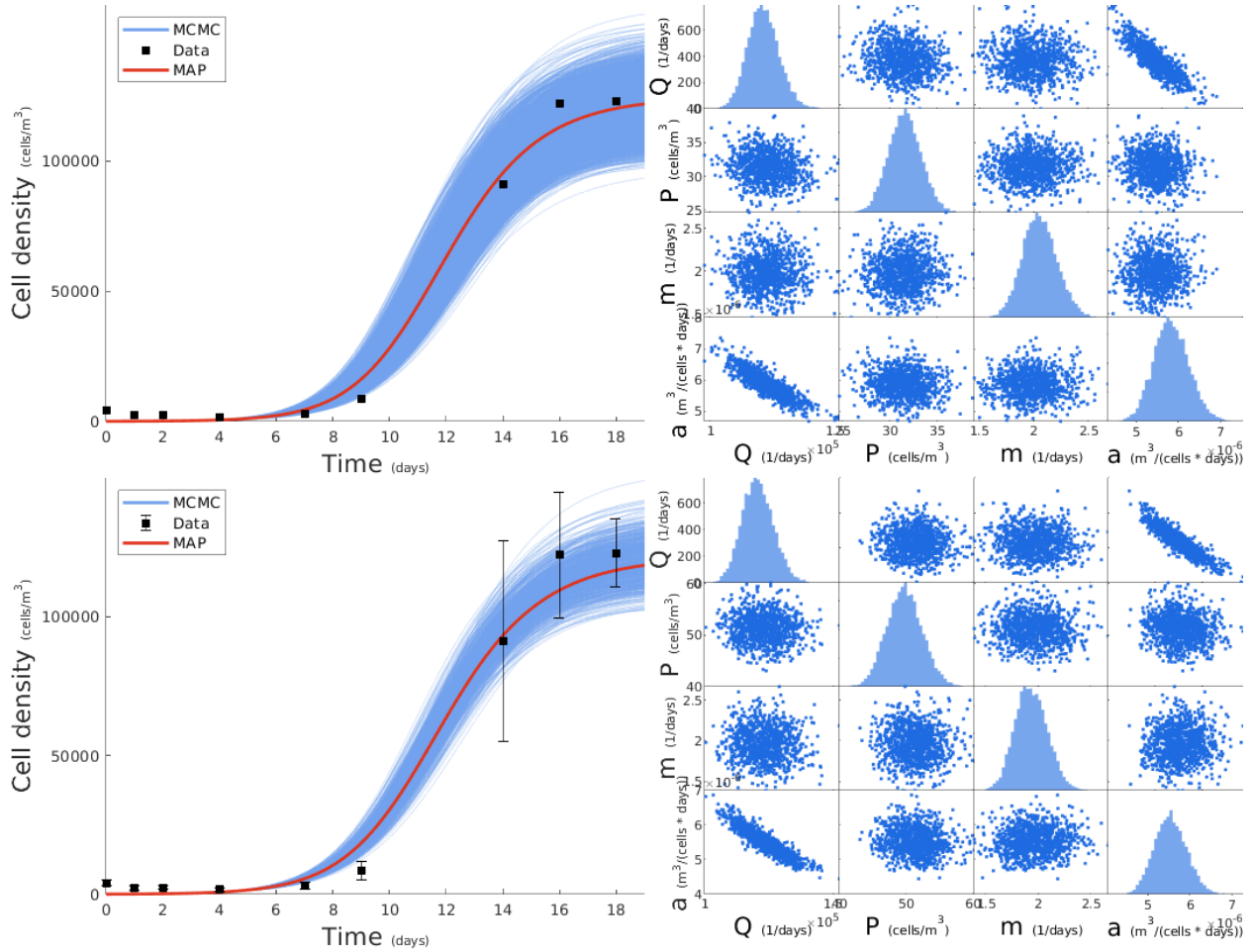


Figure 4: Fitting real data from Pro experiments. The first row shows our results for a linear constraint and the second row shows our results for a quadratic constraint. (top and bottom left) We use our MCMC sampled parameter values to generate thousands of ODE solutions which are plotted as the blue curves, we then use the MAP estimate to generate the red curve and all this is compared to the data points shown as black squares. (top and bottom right) while doing the parameter estimation we can also see how well we reproduce the hidden measurements. We show scatter plots of each parameter compared with the other in the off-diagonal panels. On the diagonal panels we show the histogram created by thousands of MCMC samples of each parameter.

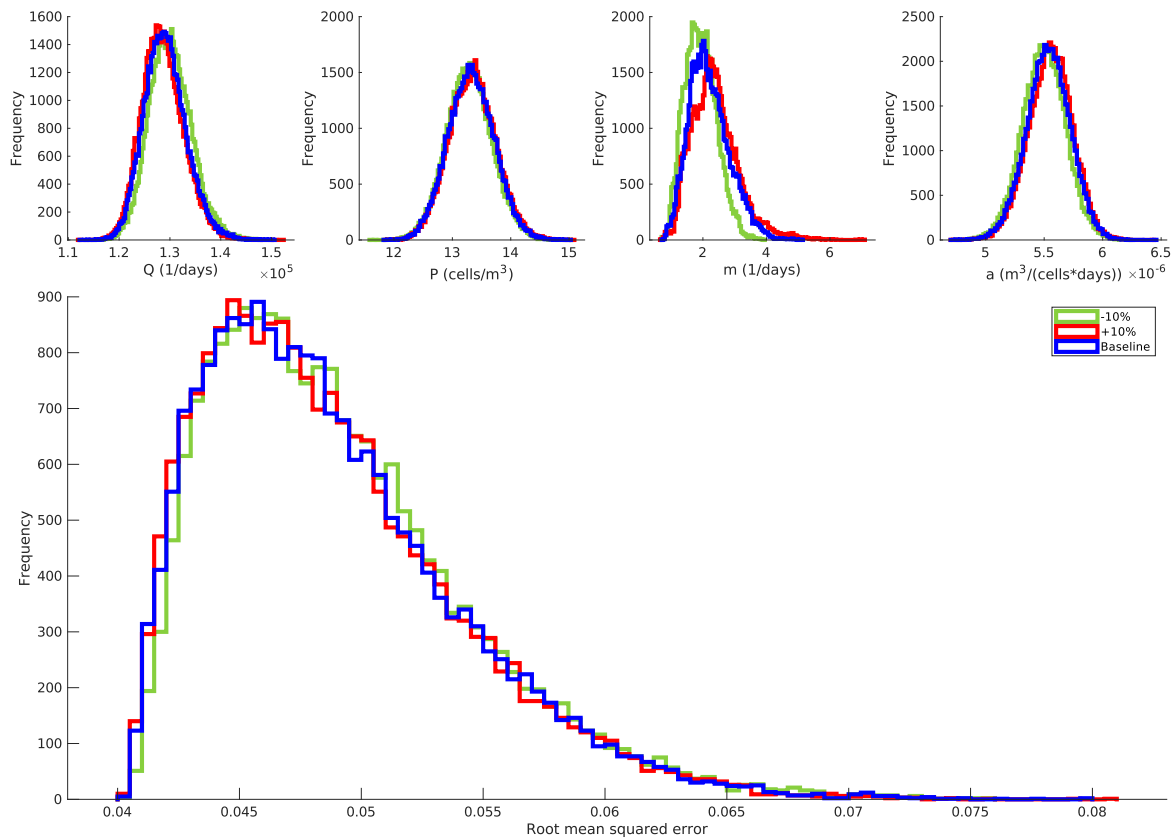


Figure 5: Sensitivity analysis of our model's hyper-parameters for Q, P, m, a . To evaluate the sensitivity, we change the values of the hyperparameter $\psi_Q, \psi_P, \psi_m, \psi_a$ from a baseline (blue) to an increase (red) of 10% and a decrease (green) of 10%. In the upper panels, we show marginal posteriors for each parameter across the three cases. In the lower panel, we show the root mean squared error (RMSE) when we compare our MCMC trajectories from the three different cases with the data. Across all the figures, we see a significant overlap of the three cases, indicating that our methods are not sensitive to changes in the hyper-parameter values.

experiments conducted on *Prochlorococcus* populations and a specialized dynamical system representing the underlying behavior. Nevertheless, the generality of our method allows for applications involving diverse data sets or dynamical models.

Due to its robustness, our methods can contribute to principled learning and assimilation efforts in IVPs where the underlying measurements are hidden, missing, or distorted by non-Gaussian noise and aggregation. These features are critical for extracting reliable insights from historical data sets or data sets that are confidential or obfuscated, and only down-sampled data or summary statistics are available. Using our advanced learning approach, our methods provide modelers and practitioners with enhanced tools to decipher incomplete data, ensuring the validity of their analysis despite the lack of pre-aggregated information. Our approach not only strengthens the accuracy of the inference that can be drawn, but also facilitates broader applications in the life sciences [61, 25, 39].

Our novel framework leverages the Bayesian paradigm to unify all aspects of modeling biological dynamics under uncertainty within a single posterior distribution [51]. Our comprehensive approach allows simultaneous parameter estimation, recovery of lost information, and interpretation in physical terms; however, its improved performance comes with its drawbacks. In particular, our framework entails a complex statistical learning approach that requires an extensive mathematical background and advanced computational procedures that pose a barrier to practitioners. In addition, successful implementation of our framework cannot avoid costly algorithms, such as the numerical integration of the underlying ODE, or, similar to all methods based on MCMC, repetitive generation of random variates leading to generally long runs even under the efficient sampling schemes developed herewith. Characteristically, the generation of the results in each analysis of this study requires runs of ≈ 10 hr on a typical single-core laptop computer. Reducing such a high computational time is the focus of future research that may consider specialized algorithmic improvements within problem-specific domains.

Conflict of interest

The authors declare no conflict of interest.

Acknowledgments

This work is based on raw data provided by Erik Zinser through experimental work supported by the NSF OCE-2023680 grant.

Author contributions

SM, DM, IS developed statistical methods and wrote the manuscript. DT and KM commented on the manuscript. SM contributed to the mathematical formulation and software of mESS. DM contributed to the mathematical formulation and software of cHMC. BC and EZ provided the experimental batch culture data. IS oversaw all aspects of the project.

References

- [1] Waleed Almutiry, Vineetha Warriyar KV, and Rob Deardon. Continuous time individual-level models of infectious disease: Package `epiilmct`. *Journal of Statistical Software*, 98:1–44, 2021.
- [2] Hans C. Andersen. Rattle: a "velocity" version of the shake algorithm for molecular dynamics calculations. *Journal of Computational Physics*, 52:24–34, 1983.
- [3] Kendall Atkinson. *An introduction to numerical analysis*. John wiley & sons, 1991.
- [4] Paul M Berube, Steven J Biller, Alyssa G Kent, Jessie W Berta-Thompson, Sara E Roggensack, Kathryn H Roache-Johnson, Marcia Ackerman, Lisa R Moore, Joshua D Meisel, Daniel Sher, et al. Physiology and evolution of nitrate acquisition in *prochlorococcus*. *The ISME journal*, 9(5):1195–1207, 2015.
- [5] Michael Betancourt. A conceptual introduction to Hamiltonian Monte Carlo. *arXiv preprint arXiv:1701.02434*, 2017.
- [6] Steven J Biller, Paul M Berube, Debbie Lindell, and Sallie W Chisholm. *Prochlorococcus*: the structure and function of collective diversity. *Nature Reviews Microbiology*, 13(1):13–27, 2015.
- [7] Christopher M. Bishop and N. M. Nasrabadi. *Pattern Recognition and Machine Learning*. Springer, 2006.
- [8] S. Brooks, A. Gelman, and X. Meng, editors. *Handbook of Markov Chain Monte Carlo*. CRC Press, 2011.
- [9] Marcus Brubaker, Mathieu Salzmann, and Raquel Urtasun. A family of MCMC methods on implicitly defined manifolds. In *Artificial intelligence and statistics*, pages 161–172. PMLR, 2012.
- [10] Alberto Cabezas and Christopher Nemeth. Transport elliptical slice sampling. In *International Conference on Artificial Intelligence and Statistics*, pages 3664–3676. PMLR, 2023.
- [11] Benjamin C Calfee, Liz D Glasgo, and Erik R Zinser. *Prochlorococcus* exudate stimulates heterotrophic bacterial competition with rival phytoplankton for available nitrogen. *MBio*, 13(1):e02571–21, 2022.
- [12] Janet W Campbell. The lognormal distribution as a model for bio-optical variability in the sea. *Journal of Geophysical Research: Oceans*, 100(C7):13237–13254, 1995.
- [13] Janet W Campbell. The lognormal distribution as a model for bio-optical variability in the sea. *Journal of Geophysical Research: Oceans*, 100(C7):13237–13254, 1995.
- [14] Kent K Cavender-Bares, Sheila L Frankel, and Sallie W Chisholm. A dual sheath flow cytometer for ship-board analyses of phytoplankton communities from the oligotrophic oceans. *Limnology and oceanography*, 43(6):1383–1388, 1998.
- [15] William AV Clark and Karen L Avery. The effects of data aggregation in statistical analysis. *Geographical Analysis*, 8(4):428–438, 1976.

- [16] Jesús Díaz García, Pere Brunet Crosa, Isabel Navazo Álvaro, and Pere Pau Vázquez Alcocer. Downsampling methods for medical datasets. In *Proceedings of the International conferences Computer Graphics, Visualization, Computer Vision and Image Processing 2017 and Big Data Analytics, Data Mining and Computational Intelligence 2017: Lisbon, Portugal, July 21-23, 2017*, pages 12–20. IADIS Press, 2017.
- [17] Pedro Flombaum, José L Gallegos, Rodolfo A Gordillo, José Rincón, Lina L Zabala, Nianzhi Jiao, David M Karl, William KW Li, Michael W Lomas, Daniele Veneziano, et al. Present and future global distributions of the marine cyanobacteria prochlorococcus and synechococcus. *Proceedings of the National Academy of Sciences*, 110(24):9824–9829, 2013.
- [18] Andrew Gelman, John B Carlin, Hal S Stern, and Donald B Rubin. *Bayesian data analysis*. Chapman and Hall/CRC, 1995.
- [19] H. Goldstein, C. Poole, and J. Safko. *Classical Mechanics*. Addison-Wesley, 1980.
- [20] Benjamin Haibe-Kains, George Alexandru Adam, Ahmed Hosny, Farnoosh Khodakarami, Massive Analysis Quality Control (MAQC) Society Board of Directors Shraddha Thakkar 35 Kusko Rebecca 36 Sansone Susanna-Assunta 37 Tong Weida 35 Wolfinger Russ D. 38 Mason Christopher E. 39 Jones Wendell 40 Dopazo Joaquin 41 Furlanello Cesare 42, Levi Waldron, Bo Wang, Chris McIntosh, Anna Goldenberg, Anshul Kundaje, et al. Transparency and reproducibility in artificial intelligence. *Nature*, 586(7829):E14–E16, 2020.
- [21] Ernst Hairer, Christian Lubich, and Gerhard Wanner. *Geometric Numerical Integration: Structure-Preserving Algorithms for Ordinary Differential Equations*. Springer, second edition, 2006.
- [22] Emil Heesche and Mette Asmild. Implications of aggregation uncertainty in data envelopment analysis: An application in incentive regulation. *Decision Analytics Journal*, 4:100103, 2022.
- [23] Audra Hinson, Spiro Papoulis, Lucas Fiet, Margaret Knight, Priscilla Cho, Brielle Szeltner, Ioannis Sgouralis, and David Talmy. A model of algal-virus population dynamics reveals underlying controls on material transfer. *Limnology and Oceanography*, 68(1):165–180, 2023.
- [24] Hanwen Huang, Andreas Handel, and Xiao Song. A bayesian approach to estimate parameters of ordinary differential equation. *Computational statistics*, 35:1481–1499, 2020.
- [25] Yu Jiang, Sai Chen, Daniel McGuire, Fang Chen, Mengzhen Liu, William G Iacono, John K Hewitt, John E Hokanson, Kenneth Krauter, Markku Laakso, et al. Proper conditional analysis in the presence of missing data: Application to large scale meta-analysis of tobacco use phenotypes. *PLoS genetics*, 14(7):e1007452, 2018.
- [26] Heather SL Jim, Aasha I Hoogland, Naomi C Brownstein, Anna Barata, Adam P Dicker, Hans Knoop, Brian D Gonzalez, Randa Perkins, Dana Rollison, Scott M Gilbert, et al. Innovations in research and clinical care using patient-generated health data. *CA: a cancer journal for clinicians*, 70(3):182–199, 2020.
- [27] Zackary I Johnson, Erik R Zinser, Allison Coe, Nathan P McNulty, E Malcolm S Woodward, and Sallie W Chisholm. Niche partitioning among prochlorococcus ecotypes along ocean-scale environmental gradients. *Science*, 311(5768):1737–1740, 2006.

- [28] Yunbum et al Kook. Sampling with Riemannian Hamiltonian Monte Carlo in a constrained space. *Proceedings of the 36th Conference on Neural Processing Systems*, 2022.
- [29] Jeffrey C Lagarias, James A Reeds, Margaret H Wright, and Paul E Wright. Convergence properties of the nelder–mead simplex method in low dimensions. *SIAM Journal on optimization*, 9(1):112–147, 1998.
- [30] Kody Law, Andrew Stuart, and Kostas Zygalakis. Data assimilation. *Cham, Switzerland: Springer*, 214:52, 2015.
- [31] Antony Lee, Konstantinos Tsekouras, Christopher Calderon, Carlos Bustamante, and Steve Pressé. Unraveling the thousand word picture: an introduction to super-resolution data analysis. *Chemical reviews*, 117(11):7276–7330, 2017.
- [32] Peter M Lee. *Bayesian statistics*. Oxford University Press London:, 1989.
- [33] B. Leimkuhler and S. Reich. Symplectic integration of constrained Hamiltonian systems. *Mathematics of Computation*, 63(208):589–605, October 1994.
- [34] Benedict Leimkuhler and Sebastian Reich. *Simulating Hamiltonian Dynamics*. Cambridge University Press, 2004.
- [35] Tony Lelièvre, Mathias Rousset, and Gabriel Stoltz. Hybrid Monte Carlo methods for sampling probability measures on submanifolds. *Numerische Mathematik*, 143:379–421, 2019.
- [36] Nathaniel J Linden, Boris Kramer, and Padmini Rangamani. Bayesian parameter estimation for dynamical models in systems biology. *PLOS Computational Biology*, 18(10):e1010651, 2022.
- [37] J. S. Liu. *Monte Carlo Strategies in Scientific Computing*. Springer, 2001.
- [38] Tim Maiwald, Helge Hass, Bernhard Steiert, Joep Vanlier, Raphael Engesser, Andreas Raue, Friederike Kipkeew, Hans H Bock, Daniel Kaschek, Clemens Kreutz, et al. Driving the model to its limit: profile likelihood based model reduction. *PloS one*, 11(9):e0162366, 2016.
- [39] Jeanet Mante, Nishanthi Gangadharan, David J Sewell, Richard Turner, Ray Field, Stephen G Oliver, Nigel Slater, and Duygu Dikicioglu. A heuristic approach to handling missing data in biologics manufacturing databases. *Bioprocess and biosystems engineering*, 42:657–663, 2019.
- [40] Katherine Markham, Amy E Frazier, Kunwar K Singh, and Marguerite Madden. A review of methods for scaling remotely sensed data for spatial pattern analysis. *Landscape Ecology*, 38(3):619–635, 2023.
- [41] Adam C Martiny, Lanying Ma, Céline Mougnot, Jeremy W Chandler, and Erik R Zinser. Interactions between thermal acclimation, growth rate, and phylogeny influence prochlorococcus elemental stoichiometry. *PLoS One*, 11(12):e0168291, 2016.
- [42] Nicholas Metropolis, Arianna W Rosenbluth, Marshall N Rosenbluth, Augusta H Teller, and Edward Teller. Equation of state calculations by fast computing machines. *The journal of chemical physics*, 21(6):1087–1092, 1953.

- [43] Lisa R Moore, Allison Coe, Erik R Zinser, Mak A Saito, Matthew B Sullivan, Debbie Lindell, Katya Frois-Moniz, John Waterbury, and Sallie W Chisholm. Culturing the marine cyanobacterium prochlorococcus. *Limnology and Oceanography: Methods*, 5(10):353–362, 2007.
- [44] J Jeffrey Morris, Zackary I Johnson, Martin J Szul, Martin Keller, and Erik R Zinser. Dependence of the cyanobacterium prochlorococcus on hydrogen peroxide scavenging microbes for growth at the ocean’s surface. *PloS one*, 6(2):e16805, 2011.
- [45] J Jeffrey Morris, Robin Kirkegaard, Martin J Szul, Zackary I Johnson, and Erik R Zinser. Facilitation of robust growth of prochlorococcus colonies and dilute liquid cultures by “helper” heterotrophic bacteria. *Applied and environmental microbiology*, 74(14):4530–4534, 2008.
- [46] Ryan J Murphy, Oliver J Maclaren, and Matthew J Simpson. Implementing measurement error models with mechanistic mathematical models in a likelihood-based framework for estimation, identifiability analysis and prediction in the life sciences. *Journal of the Royal Society Interface*, 21(210):20230402, 2024.
- [47] Iain Murray, Ryan Adams, and David MacKay. Elliptical slice sampling. In *Proceedings of the thirteenth international conference on artificial intelligence and statistics*, pages 541–548. JMLR Workshop and Conference Proceedings, 2010.
- [48] Radford M Neal. Mcmc using hamiltonian dynamics. *arXiv preprint arXiv:1206.1901*, 2012.
- [49] Guy H Orcutt, Harold W Watts, and John B Edwards. Data aggregation and information loss. *The American Economic Review*, 58(4):773–787, 1968.
- [50] Fred Partensky, Wolfgang R Hess, and Daniel Vaultot. Prochlorococcus, a marine photosynthetic prokaryote of global significance. *Microbiology and molecular biology reviews*, 63(1):106–127, 1999.
- [51] Steve Pressé and Ioannis Sgouralis. *Data Modeling for the Sciences: Applications, Basics, Computations*. Cambridge University Press, 2023.
- [52] Alfio Quarteroni, Riccardo Sacco, and Fausto Saleri. *Numerical mathematics*, volume 37. Springer Science & Business Media, 2006.
- [53] Sebastian Reich and Colin Cotter. *Probabilistic forecasting and Bayesian data assimilation*. Cambridge University Press, 2015.
- [54] Christian P. Robert and G. Casella. *Monte Carlo Statistical Methods*. Springer, 1999.
- [55] Weston C Roda. Bayesian inference for dynamical systems. *Infectious Disease Modelling*, 5:221–232, 2020.
- [56] Tom Ronan, Zhijie Qi, and Kristen M Naegle. Avoiding common pitfalls when clustering biological data. *Science signaling*, 9(432):re6–re6, 2016.
- [57] Lawrence F Shampine and Mark W Reichelt. The matlab ode suite. *SIAM journal on scientific computing*, 18(1):1–22, 1997.
- [58] Devinderjit Sivia and John Skilling. *Data analysis: a Bayesian tutorial*. OUP Oxford, 2006.

- [59] Vinayak Smith, Densearn Seo, Ritesh Warty, Olivia Payne, Mohamed Salih, Ken Lee Chin, Richard Ofori-Asenso, Sathya Krishnan, Fabricio da Silva Costa, Beverley Vollenhoven, et al. Maternal and neonatal outcomes associated with covid-19 infection: A systematic review. *Plos one*, 15(6):e0234187, 2020.
- [60] Josef Stoer, Roland Bulirsch, R Bartels, Walter Gautschi, and Christoph Witzgall. *Introduction to numerical analysis*, volume 1993. Springer, 1980.
- [61] Sandra Taylor, Matthew Ponzini, Machel Wilson, and Kyoungmi Kim. Comparison of imputation and imputation-free methods for statistical analysis of mass spectrometry data with missing data. *Briefings in Bioinformatics*, 23(1):bbab353, 2022.
- [62] A Franciscus van der Meer, Marco AE Marcus, Daniël J Touw, Johannes H Proost, and Cees Neef. Optimal sampling strategy development methodology using maximum a posteriori bayesian estimation. *Therapeutic drug monitoring*, 33(2):133–146, 2011.
- [63] Atheendar S Venkataramani, Rourke O’Brien, Gregory L Whitehorn, and Alexander C Tsai. Economic influences on population health in the united states: toward policymaking driven by data and evidence. *PLoS medicine*, 17(9):e1003319, 2020.
- [64] Franz-Georg Wieland, Adrian L Hauber, Marcus Rosenblatt, Christian Tönsing, and Jens Timmer. On structural and practical identifiability. *Current Opinion in Systems Biology*, 25:60–69, 2021.
- [65] Paula R Williamson, Catrin Tudur Smith, Jane L Hutton, and Anthony G Marson. Aggregate data meta-analysis with time-to-event outcomes. *Statistics in medicine*, 21(22):3337–3351, 2002.
- [66] Samantha L Wilson, Gregory P Way, Wout Bittremieux, Jean-Paul Armache, Melissa A Haendel, and Michael M Hoffman. Sharing biological data: why, when, and how. *FEBS letters*, 595(7):847, 2021.
- [67] Fangfang Xia, Jonathan Allen, Prasanna Balaprakash, Thomas Brettin, Cristina Garcia-Cardona, Austin Clyde, Judith Cohn, James Doroshov, Xiaotian Duan, Veronika Dubinkina, et al. A cross-study analysis of drug response prediction in cancer cell lines. *Briefings in bioinformatics*, 23(1):bbab356, 2022.
- [68] Xiangyu Xu, Muchen Li, Wenxiu Sun, and Ming-Hsuan Yang. Learning spatial and spatio-temporal pixel aggregations for image and video denoising. *IEEE Transactions on Image Processing*, 29:7153–7165, 2020.
- [69] Erik R Zinser, Debbie Lindell, Zackary I Johnson, Matthias E Futschik, Claudia Steglich, Maureen L Coleman, Matthew A Wright, Trent Rector, Robert Steen, Nathan McNulty, et al. Choreography of the transcriptome, photophysiology, and cell cycle of a minimal photoautotroph, prochlorococcus. *PloS one*, 4(4):e5135, 2009.

A Summary of the framework's equations

In its most general form, our framework is described by:

$$g \sim \mathbb{C} \tag{19}$$

$$h \sim \mathbb{B} \tag{20}$$

$$y_n^k | g, h \sim \mathbb{A}(F(x^g(t_n)), h) \quad k = 1, \dots, K, \quad n = 1, \dots, N \tag{21}$$

$$z_n | y_n^{1:K} \sim \delta_{G(y_n^{1:K})} \quad n = 1, \dots, N \tag{22}$$

where \mathbb{B}, \mathbb{C} are prior distributions of the dynamical g and observation h parameters, \mathbb{A} is the likelihood of the raw measurements $y_{1:N}^{1:M}$, $F(\cdot)$ is the observation function, and $x^g(\cdot)$ is the solution of the underlying IVP. In this description, the aggregated data is $z_{1:N}^{1:M}$, the evaluation times are $t_{1:N}$, the statistics are $G^{1:M}(\cdot)$, and the batch size is K .

B Definitions of probability distributions

Here we present the parameterization of the probability distributions that we use throughout this study.

- The *Log Normal* has probability density given by

$$\text{LogNormal}(y; x, h) = \frac{1}{y} \sqrt{\frac{h}{2\pi}} \exp\left(-\frac{h}{2} \left(\log \frac{y}{x}\right)^2\right)$$

with x being the median and h being the precision.

- The *Gamma* has probability density given by

$$\text{Gamma}(\gamma; \kappa, \theta) = \frac{\gamma^{\kappa-1} e^{-\gamma/\theta}}{\Gamma(\kappa) \theta^\kappa}$$

this has mean $\kappa\theta$.

- The *Delta* density is given by

$$\delta_a(E) = \begin{cases} 1 & \text{if } a = E \\ 0 & \text{if } a \neq E \end{cases}$$

C Computational methods

C.1 Multiplicative elliptical slice sampling

To sample from a generic target with probability density $\pi(g_{1:M})$ over a continuous multivariate random variable $g_{1:M}$, we start by completing with normal auxiliary variables $\lambda_{1:M}$, which are independent from our parameters

$$\lambda_m \sim \text{Normal}(0, \sigma_m^2), \quad m = 1, \dots, M.$$

After this completion, our target becomes $p(g_{1:M}, \lambda_{1:M})$. At this stage, we continue with a 2-step Gibbs sampler consisting of:

- Obtain $\lambda_{1:M}$ by sampling from $p(\lambda_{1:M}|g_{1:M})$. Due to the independence between $\lambda_{1:M}$ and $g_{1:M}$, this step is achieved by direct sampling normal variates.
- Apply a change of variables $(g_{1:M}, \lambda_{1:M}) \mapsto (\phi_{1:M}, \psi_{1:M})$ defined by

$$\begin{aligned} \phi_m &= g_m \exp(\psi_m), \\ \psi_m &= \lambda_m. \end{aligned}$$

to obtain a transformed target. According to [51], this is given by

$$p(\phi_{1:M}, \psi_{1:M}) \propto \pi(g_{1:M}) \exp\left(-\sum_{m=1}^M \lambda_m\right) \prod_{m=1}^M \text{Normal}(\lambda_m; 0, \sigma_m^2).$$

- Resample $\psi_{1:M}$ from $p(\psi_{1:M}|\phi_{1:M})$. Due to the latent Gaussian form of the transformed target $p(\phi_{1:M}, \psi_{1:M})$, this is achieved using the elliptical slice sampler [47, 10, 48].
- Recover the original variables $g_{1:M}$ using the inverse transform $(\phi_{1:M}, \psi_{1:M}) \mapsto (g_{1:M}, \lambda_{1:M})$ given by

$$g_m = \phi_m \exp(-\psi_m).$$

Our entire scheme, including the elliptical slice sampling stage, is implemented in algorithm 1.

C.2 Standard Hamiltonian Monte Carlo

The HMC algorithm is an MCMC method for sampling a target distribution with density $\pi(q) \propto f(q)$ known only up to a multiplicative constant. We assume that the support Q of $f(q)$ is a Euclidean space of fixed dimension. HMC is an extension of the Metropolis algorithm, but with a proposal rule constructed in analogy with classical Hamiltonian mechanics, the dynamics of which are energy conserving, reversible, and measure preserving [21, 19]. Here, the sequence of samples $\{q^{(j)}\}_{j=0:J}$ produced by HMC is viewed as a sequence of positions of a particle, or of an ensemble of particles, governed by Hamiltonian dynamics. This analogy introduces auxiliary “momentum” variables $\{p^{(j)}\}_{j=0:J}$ and a “total energy” Hamiltonian function

$$H(q, p) = V(q) + K(p), \quad (23)$$

Algorithm 1 Multiplicative Elliptical Slice Sampler

Input: Current state \mathbf{g} , auxiliary variance σ^2 , likelihood function L

Output: New state \mathbf{g}'

$\nu \sim \mathcal{N}(0, S)$

▷ Choose ellipse

$\lambda \sim \mathcal{N}(0, \sigma^2)$

▷ Choose auxiliary variable

$u \sim \text{Uniform}(0, 1)$

$\log y \leftarrow \log L(\mathbf{g}) + \log u$

▷ Set log-likelihood threshold

$\theta \sim \text{Uniform}(0, 2\pi)$

▷ Draw an initial proposal

$[\theta_{\min}, \theta_{\max}] \leftarrow [\theta - 2\pi, \theta]$

▷ Define a bracket

while true do

$\lambda' \leftarrow \lambda \cos \theta + \nu \sin \theta$

▷ Traverse auxiliary space with ellipse

$\mathbf{g}' \leftarrow \mathbf{g} * \exp(\lambda - \lambda')$

▷ Reverse CoV

if $\log L(\mathbf{g}') + \sum \lambda > \log y + \sum \lambda'$ **then**

▷ Accept

return \mathbf{g}'

else

if $\theta < 0$ **then**

$\theta_{\min} \leftarrow \theta$

else

$\theta_{\max} \leftarrow \theta$

end if

$\theta \sim \text{Uniform}(\theta_{\min}, \theta_{\max})$

▷ Shrink the bracket and try a new point

end if

end while

where we define, by analogy, a “potential energy” function

$$V(q) = -\log f(q), \quad (24)$$

and a “kinetic energy” function

$$K(p) = \frac{1}{2} p^T M^{-1} p, \quad (25)$$

where M is a “mass” matrix. This choice for the Hamiltonian function leverages the known gradient information of our target distribution $\pi(q)$ [5, 8]. We can convert our proportionality relationship

$$\pi(q) \propto f(q) \quad (26)$$

into an equality involving the gradient of our target distribution,

$$\nabla \log f(q) = -\nabla V(q). \quad (27)$$

So the method is, given a sample $q^{(j)}$, generate a proposal sample by evolving dynamics on phase space $((q, p)$ -space) governed by Hamilton’s equations, which are, in this case,

$$\dot{q} = M^{-1} p, \quad q(0) = q^{(j)}, \quad (28)$$

$$\dot{p} = \nabla \log f(q), \quad p(0) = p^{(j)}. \quad (29)$$

We integrate these dynamics for a fixed time, either exactly or approximately, and denote by

$$\left(\tilde{q}^{(j+1)}, \tilde{p}^{(j+1)}\right) = \Phi\left(q^{(j)}, p^{(j)}\right) \quad (30)$$

the result of the integration. Here, $q^{(j)}$ is carried over from the previous sampling step and $p^{(j)}$ follows the sampling rule

$$p^{(j)} \sim \mathcal{N}(0, M), \quad (31)$$

where $\mathcal{N}(0, M)$ is a multivariate normal. For the Metropolis step, we compute the acceptance ratio $R^{(j)}$ using the expression

$$R^{(j)} = \exp\left(H\left(q^{(j)}, p^{(j)}\right) - H\left(\tilde{q}^{(j+1)}, \tilde{p}^{(j+1)}\right)\right). \quad (32)$$

As in the Metropolis algorithm, we accept the proposed sample and set $q^{(j+1)} = \tilde{q}^{(j+1)}$ with probability $\min(1, R^{(j)})$, otherwise we set $q^{(j+1)} = q^{(j)}$. We summarize the algorithm below.

Algorithm 2 Hamiltonian Monte Carlo

Input: $q^{(0)} \in Q$
Output: $\{q^{(j)}\}_{j=0:J}$
for $j=0:J-1$ **do**
 $p^{(j)} \sim \mathcal{N}(0, M)$
 $(\tilde{q}^{(j+1)}, \tilde{p}^{(j+1)}) \leftarrow \Phi(q^{(j)}, p^{(j)})$
 $\gamma \sim \text{Bernoulli}(\min(1, R^{(j)}))$
 $q^{(j+1)} \leftarrow \gamma \tilde{q}^{(j+1)} + (1 - \gamma)q^{(j)}$
end for

If the integration is exact or if a reversible, measure-preserving numerical integrator (such as Störmer-Verlet) is used, then this scheme satisfies a detailed balance [5], so the empirical statistics of the resulting Markov chain $\{q^{(j)}\}_{j=0:J}$ approach those of the target distribution with density $\pi(q)$.

In practice the exact integration of the Hamiltonian is not possible, but the better we can approximately integrate the Hamiltonian, the higher our acceptance rate will be [8, 5]. The standard numerical integrator for HMC is the explicit, second order Störmer-Verlet numerical scheme [37, 8, 5]. As it is the base algorithm from which RATTLE is derived, we give one step (step size h) of the Störmer-Verlet numerical scheme here.

Algorithm 3 Störmer-Verlet numerical integration (one step, step size h)

Input: (q, p) in phase space
Output: (\tilde{q}, \tilde{p})
 $\bar{p} \leftarrow p - \frac{h}{2} \nabla V(q)$
 $\tilde{q} \leftarrow q + h \nabla K(\bar{p})$
 $\tilde{p} \leftarrow \bar{p} - \frac{h}{2} \nabla V(\tilde{q})$

The Störmer-Verlet scheme is indeed reversible and preserves the phase-space measure, so the resulting Markov chain has the desired approximation properties.

C.3 Constrained Hamiltonian Monte Carlo

In this section, we follow the notation used in the previous section and outline the constrained Hamiltonian Monte Carlo algorithm as described by Brubaker et al. [9]. The goal of cHMC is to sample a surface measure, in particular a probability distribution with density $\pi(q) \propto f(q)$ known only up to a multiplicative constant supported on a differentiable manifold \mathcal{M} . We take \mathcal{M} to be embedded in Euclidean space and defined as the zero set of a constraint function $q \mapsto c(q) \in \mathbb{R}^d$ with full-rank Jacobian $J_{c(q)}$ for all $q \in \mathcal{M}$. We will use the notation $\nabla c(q) = J_{c(q)}^T$ in analogy to the gradient for the transpose of the Jacobian. As in the unconstrained setting, we introduce a virtual momentum variable p .

To represent data aggregation, the set of values $q = y_{1:N}^{1:K}$ which simultaneously satisfy eq. (1) is parametrized as the solution set of the following $2N$ constraint functions, $G^1(y_n^{1:K}) = z_n^1$ and $G^2(y_n^{1:K}) = z_n^2$ for $n = 1 : N$, where z_n^1 and z_n^2 are the mean and variance, respectively, of the K measurements taken at time t_n . Here, G^1 and G^2 are as defined in eqs. (2) and (3). It is convenient for the implementation to reparametrize these $2N$ constraints as follows. We constrain samples $q = y_{1:N}^{1:K}$ to lie on the zero locus of

$$c_n^1(q) = \frac{1}{K} \sum_{k=1}^K y_n^k - z_n^1, \quad n = 1 : N, \quad (33)$$

$$c_n^2(q) = \frac{1}{K} \sum_{k=1}^K (y_n^k)^2 - \tilde{z}_n^2 \quad n = 1 : N, \quad (34)$$

where \tilde{z}_n^2 is the raw (uncentered) second moment of the K measurements recorded at time t_n . We collect all constraints into a column vector-valued function $c = (c_1^1, \dots, c_N^1, c_1^2, \dots, c_N^2)^T$ which reduces the satisfaction of the $2N$ mean and variance constraints to the simple expression $c(q) = 0$.

With this formalism, the method is defined by the following update rule. Given a sample $q^{(j)} \in \mathcal{M}$, generate a proposal by evolving the differential algebraic equations

$$\dot{q} = M^{-1}p, \quad q(0) = q^{(j)}, \quad (35)$$

$$\dot{p} = \nabla \log f(q) - \nabla c(q)\lambda(q, p), \quad p(0) = p^{(j)}, \quad (36)$$

$$\lambda(q, p) \in \mathbb{R}^d \text{ s.t. } c(q) = 0. \quad (37)$$

Here, λ is a Lagrange multiplier used to enforce that constraint $c(q) = 0$ is satisfied throughout the trajectory. As before, $q^{(j)}$ is inherited from the previous sampling step, but now $p^{(j)}$ is a random vector sampled from a distribution depending on the geometry of the constraint manifold \mathcal{M} .

Let $T_q\mathcal{M}$ denote the plane tangent to \mathcal{M} at q , and let $\mathcal{N}^{(j)}$ denote the surface measure in $T_{q^{(j)}}\mathcal{M}$ induced by the normal distribution $\mathcal{N}(0, M)$ in the ambient Euclidean space. We take the initial momentum sample $p^{(j)}$ from the singular distribution $\mathcal{N}^{(j)}$. Under these initial conditions, the solution (q, p) remains in the tangent bundle $T\mathcal{M} = \sqcup_{q \in \mathcal{M}} T_q\mathcal{M}$ of \mathcal{M} [19, 33, 34].

We integrate these dynamics for a fixed time and denote the result by

$$\left(\tilde{q}^{(j+1)}, \tilde{p}^{(j+1)}\right) = \Psi\left(q^{(j)}, p^{(j)}\right). \quad (38)$$

The integration can be exact or approximate. We compute the Metropolis acceptance ratio $R^{(j)}$ using the same expression as in the unconstrained case. With these particulars, we can give the cHMC algorithm.

Algorithm 4 Constrained Hamiltonian Monte Carlo

Input: $q^{(0)} \in \mathcal{M}$
Output: $\{q^{(j)}\}_{j=0:J}$
for $j=0:J-1$ **do**
 $p^{(j)} \sim \mathcal{N}^{(j)}$
 $(\tilde{q}^{(j+1)}, \tilde{p}^{(j+1)}) \leftarrow \Psi(q^{(j)}, p^{(j)})$
 $\gamma \sim \text{Bernoulli}(\min(1, R^{(j)}))$
 $q^{(j+1)} \leftarrow \gamma \tilde{q}^{(j+1)} + (1 - \gamma)q^{(j)}$
end for

Since a numerical integrator with energy-conserving properties that respects the constraint structure is desired, the standard choice for a numerical integrator is the second-order method RATTLE [9, 35, 28]. In the context of molecular dynamics, it has been shown that RATTLE is reversible and preserves Lebesgue surface measure in $T\mathcal{M}$ (see [33, 34]), and hence satisfies a detailed balance. So, the Markov chain generated by cHMC has the desired statistical approximation properties. Here we describe one step of RATTLE with step size h .

Algorithm 5 RATTLE numerical integration (one step, step size h)

Input: $(q, p) \in T\mathcal{M}$
Output: (\tilde{q}, \tilde{p})
 $\tilde{p} \leftarrow p - \frac{h}{2}[\nabla V(q) + \nabla c(q)\lambda_{(q)}], \quad \lambda_{(q)} \text{ s.t. } c(q + h\nabla K(\tilde{p})) = 0$
 $\tilde{q} \leftarrow q + h\nabla K(\tilde{p})$
 $\tilde{p} \leftarrow \tilde{p} - \frac{h}{2}[\nabla V(\tilde{q}) + \nabla c(\tilde{q})\lambda_{(p)}], \quad \lambda_{(p)} \text{ s.t. } \nabla K(\tilde{p}) \cdot \nabla c(\tilde{q}) = 0$

Though based on Störmer-Verlet, the RATTLE scheme is quite computationally distinct. Each step of RATTLE requires, in general, the solving of a nonlinear and a linear system to find the appropriate multipliers $\lambda_{(q)}$ and $\lambda_{(p)}$, respectively. We implement these solvers with the Newton-Raphson method. The condition on $\lambda_{(q)}$ keeps $\tilde{q} \in \mathcal{M}$ while $\lambda_{(p)}$ keeps $\tilde{p} \in T_q\mathcal{M}$ ensuring that the output (\tilde{q}, \tilde{p}) remains in $T\mathcal{M}$.

D Least squares parameter estimation

We formulate least-squares (LS) estimation in section 2.2 as an optimization problem

$$g^* = \operatorname{argmin}_g L(g),$$

where the objective function is given by

$$L(g) = \sum_{n=1}^N (z_n - F(x^g(t_n)))^2.$$

Here, $x^g(t_n)$ denotes the solution of the IVP in eq. (5) with parameters g evaluated at time t_n , $F(\cdot)$ is the observation function in eq. (4), and z_n denotes the summary statistic computed in eq. (1).

For the numerical solution of the minimization problem, we apply a derivative-free method as implemented in the Nelder-Mead simplex algorithm [29].